Multiple Order Diffractions by Laser-Induced Transient Grating in Nematic MBBA Film

Seong Kyu Kim* and Hackjin Kim†,*

Department of Chemistry and Institute of Basic Science, Sungkyunkwan University, Suwon 440-746, Korea
†Department of Chemistry, Chungnam National University, Taejon 305-764, Korea
Received March 2, 1999

The laser-induced transient grating method is applied to study the dynamics of the nematic MBBA film. The nanosecond laser pulses of 355 nm are used to make the transient grating and the cw He-Ne laser of 633 nm is used to probe the dynamics. Strong multiple order diffractions are observed at high nematic temperatures. The reordering process induced by the phototransformed state, which is the locally melted state from the nematic sample, is attributed to the main origin of the multiple order diffractions from the nematic MBBA. The characteristics of the multiple order gratings are discussed with the grating profiles simulated from the multiple diffraction signals.

Introduction

A number of physical properties[1-3] of liquid crystals are highly anisotropic owing to intermolecular interactions strong enough to produce aligned structures. The anisotropic molecular structure is attributed to the alignment of the liquid crystalline molecules, which has been utilized in electro-optic and display devices.[4] The locally aligned structures called pseudonematic domains are maintained even in the isotropic phase of the liquid crystalline materials.[2,5,6] While the pseudonematic domains undergo dynamic changes, the size of the aligned domains is related quantitatively with the temperature. The presence of the pseudonematic domains makes the dynamics of the isotropic liquid crystal different from that of the conventional isotropic liquids. The dynamic characteristics of the isotropic phase such as the molecular orientation are described well with a theoretical model related to the pseudonematic domains.

Liquid crystals also have extraordinarily large nonlinear optical properties, as the strong intermolecular interactions produce new polarizations in a collective way under an external optical field. Anisotropic molecular shape and long conjugated electronic structure of liquid crystalline molecules contribute to the large optical nonlinearity. The collective molecular motion makes the nonlinear optical effects of liquid crystals rise in a much slower time scale than those of inorganic nonlinear materials. While many nonlinear optical methods,[3,7-12] such as self-focusing, optical phase conjugation, and four wave mixing, have been used to study the optical nonlinear properties of liquid crystals, the dynamic approach can take advantage of the temporal separation of various physical origins. Recently we have applied the transient grating method to study the nonlinear optical dynamics of MBBA (4-methoxybenzylidene-4-n-butylaniline).[11,12] In this work, we supplement the previous study[12] of the nematic MBBA with the multiple order diffractions. While MBBA is one of the most studied liquid crystalline materials,[1,3,13,14] there are many questions left unresolved in the fundamental nonlinear optical dynamics. The well-known physical properties of MBBA have been a great help to understand these complex features of the dynamics.

The transient grating method is a time-resolved version of the general four wave mixing technique.[15] In our work, two identical nanosecond laser pulses of 355 nm are overlapped at the sample to generate the transient grating interference pattern and the dynamics of the grating are probed by the diffraction of a cw He-Ne laser (633 nm). The fringe spacing of the interference pattern Λ is given by the Bragg condition.

$$\Lambda = \frac{\lambda_{ex}}{2\sin(\theta/2)} \tag{1}$$

where λ_{ex} is the wavelength of the excitation light, and θ is the beam crossing angle. The dynamics of the build-up and decay of the interference pattern provide the information on the involved physical and chemical processes.

Experimental Section

The details of our transient grating setup are found elsewhere.[11,12,16] Here we present Figure 1 that shows the directions of the optical fields and the sample alignment. We prepared planar homogeneously aligned MBBA (Tokyo Kasei, used as received) sandwiched between a pair of glasses spaced by a 170 μm thick Teflon sheet. The alignment is achieved by rubbing the glasses unidirectionally. The sample is then placed, with the preferential director axis along z-axis in Figure 1, inside a metal block that is temperature controlled within ±0.1 ^{o}C. For the grating excitation (along x-axis), two replica pulses of 355 nm from a Q-switched Nd : YAG laser are recombined at the sample. The overlap beam diameter is 3.8 mm and the irradiance of the excitation is about 10 mJ/cm^2. The cw probe beam from a 2 mW He-Ne laser is then introduced at the Bragg angle. The electric field of the excitation laser pulses has the polarization parallel to the director axis of the aligned sample and that of the probe is switchable between the parallel and the

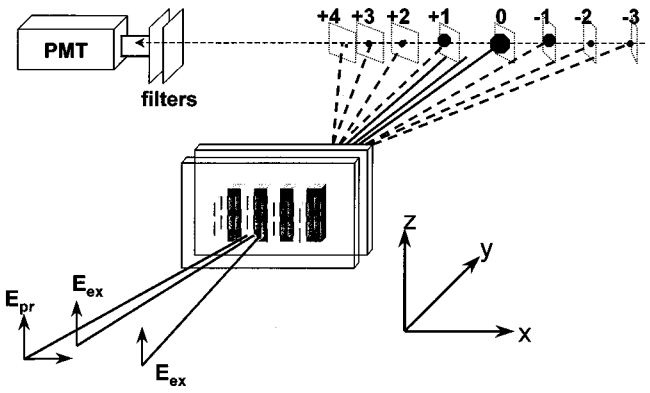

Figure 1. Directions of excitation fields (E_{ex}), probe field (E_{pr}), sample alignment, multiple diffractions of our experiment. The numbers represent the orders of the diffractions

perpendicular polarizations. The first order diffraction at all temperatures and the higher order diffractions at high nematic temperatures are observed by the naked eye. Each order diffraction beam is spatially separated and directed by a mirror into a PMT. Combinations of calibrated neutral density filters are used to scale their relative intensities. The PMT signal of the transient diffraction is recorded with a transient digitizer and averaged mathematically for 100 laser shots at the repetition rate of 1 Hz. The background signal is also obtained by blocking one of the excitation pulses, and then subtracted from the transient signal.

Results and Discussion

A. Summary of the previous work.[12] Figure 2 shows the typical decay pattern of the first order diffraction signals from the nematic MBBA film. Since the full analysis of the first order diffraction signals is given in the previous paper,[12] a summary of the important results are presented here. The diffraction signal is generally described by the squared sum of the following exponential functions;

$$I(t)=[X_1(t)+X_2(t)+X_3(t)+X_4(t)]^2 \quad (2a)$$

$$X_1(t)=A_1\exp(-t/\tau_{d1}) \quad (2b)$$

$$X_2(t)=A_2[1+\exp(-t/\tau_{r2})]\exp(-t/\tau_{d2}) \quad (2c)$$

$$X_3(t)=A_3[1+\exp(-t/\tau_{r3})]\exp(-t/\tau_{d3}) \quad (2d)$$

$$X_4(t)=A_4\exp(-t/\tau_{d4}) \quad (2e)$$

Here each X component represents the following physical origins in the order of increasing time scale; the thermal diffusion, the temperature-induced reordering, the phototransformer-induced reordering, and the mass diffusion. The best fit parameters with the above equations at the nematic temperatures are tabulated in reference 12.

The decay time constants of the first and the fourth components are proportional to the square of the fringe spacing; that is, their dynamics are diffusional and the corresponding diffusion coefficients can be determined from the fringe spacing dependence of the decay times. The thermal diffusion coefficient of MBBA is confirmed from the dynamics

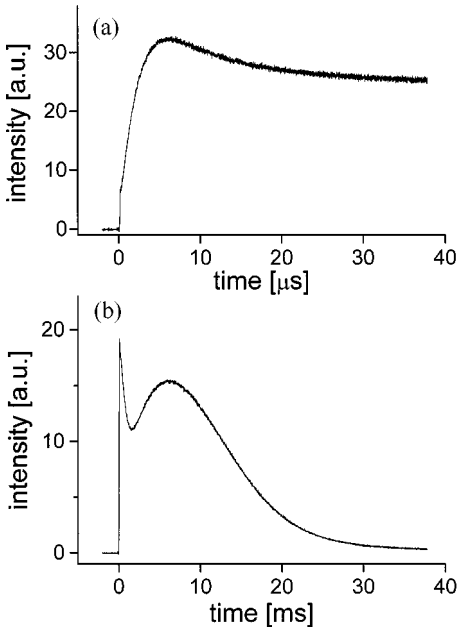

Figure 2. Typical first order diffraction signal of the nematic MBBA at 41 °C in different time scales. The probe polarization of these signals is parallel with the sample alignment and the fringe spacing is 8.0 μm. In the microsecond time scale (a), the instantaneous jump of the first component followed by an exponential decay and the rise of the second component are observed. In the millisecond time scale (b), the second component appears as an early spike, and the rise-and-decay of the third component is dominant. The fourth component is contained in the tailing.

of the first component. And the diffusion coefficient from the fourth component is confirmed as the mass diffusion of the nematic MBBA. The thermal grating is initially formed within several micrometers of the sample from the front glass since the excitation wavelength is in the strong absorption.[12] Under this excitation condition, a large thermal gradient along y-axis is initially produced. However, a very fast (*ca.* 100 ns) heat dissipation into the front glass proceeds as the thermal conductivity of glass is greater by several orders of magnitude than that of MBBA. As a result, a normal thermal diffusion along the grating wave vector that can be described by the exponential decay law follows after 1 μs. The thermal diffusion part shows a nearly complete anisotropic dependence on the probe polarization at the nematic temperatures.

The order parameter of the nematic phase is a function of temperature, and the refractive index changes as the order parameter changes with temperature. The second component, X_2 results from the fluctuation of the order parameter induced by the temperature change. The rise-and-decay of the third component X_3 becomes slower with the temperature rise and dominates near the nematic-isotropic phase transition temperature. Pinkevich *et al.*[17] showed theoretically that the large optical nonlinearity near the transition temperature can be produced from phototransformed states. The third component is considered to come from the fluctuation of the order parameter induced by the phototransformed

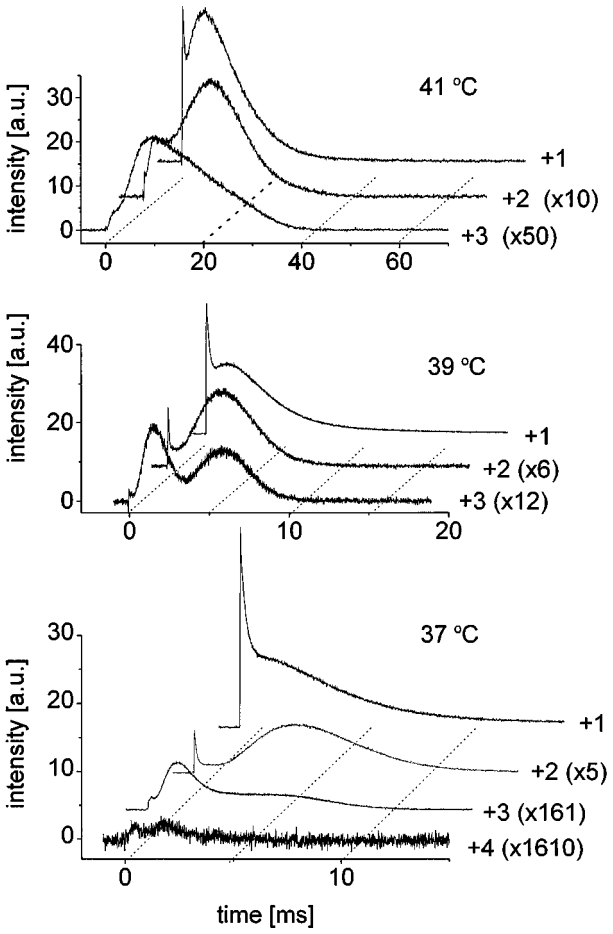

Figure 3. The multiple order diffraction signals. The fringe spacing is 7.8 m and the excitation laser power is the same as for signal of Figure 2. The numbers represent the orders of the diffraction and the numbers in the parentheses represent the relative intensity scales to the first order diffraction signal.

state. The diffraction signal dependence on the excitation laser power suggests strongly that the phototransformed state from the nematic MBBA responsible for the third component is a melted state rather than a photoisomer.

B. Grating theories for multiple order diffractions. Figure 3 illustrates the multiple order diffraction signals. There appears a small spike in the very early part of the second order diffraction signals at 37 and 39 °C. We believe that this feature is related to the evolution of the grating shape due to the second component of the first order diffraction, the temperature-induced reordering, because its submillisecond time scale corresponds to that of the X_2 of Eq. (2). This spike feature is absent in the third order diffraction signals at 37 and 39 °C and in any higher order diffractions at higher temperatures than 40 °C. Overall, the higher order diffractions show stronger features in the milliseconds than in the submilliseconds. Therefore, the reordering process due to the phototransformed state, X_3 of Eq. (2), is the most responsible for the high order diffractions. More details of the phototransformed state, or the locally melted state, are discussed later.

The phase grating theories[18-20] predict that multiple diffractions can be observed either when the grating thickness is in the thin limit or when the grating is nonsinusoidal along the wave vector. The refractive index modulation for the nonsinusoidal grating shape, Δn, can be expressed by a sum of the fourier components of the multiple order harmonics. That is,

$$\Delta n = \delta n_1 \cos(qx) + \delta n_2 \cos(2qx + \phi_2) + \delta n_3 \cos(3qx + \phi_3) + \cdots \quad (3a)$$

where δn's are the refractive index differences of the peak and the null of the corresponding harmonic gratings; $\delta n = n(\text{peak}) - n(\text{null})$, q is the wave vector of the fundamental grating; $q = 2\pi / \Lambda$, and ϕ's are the phase differences between the first order grating and the corresponding higher order grating. Since the initial excitation depth of our experiment is similar with the fringe spacing of the grating, the applicability of the thin grating limit should first be speculated. In the thin phase grating limit, the multiple diffractions can be produced even from the sinusoidal grating (*i.e.* $\delta n_2 = \delta n_3 = \cdots = 0$). In this case, the intensity of the m-th order diffraction I_m is proportional to the square of m-th order Bessel function of the first kind.[18] That is

$$I_m \propto J_m^2(2\gamma_1),\ m = \pm 1, \pm 2, \pm 3, \cdots \quad (4)$$

where $2\gamma_1$ is the argument of the Bessel function J_m and is proportional to the grating modulation δn_1. As the refractive index modulation is expected to be sufficiently small (less than 10^{-3}), each order Bessel function is nearly linear with the argument. So the intensity of the m-th order diffraction is approximately proportional to $C_m \delta n_1^2$, where the proportionality constant C_m can be approximated to the square of Bessel function maximum and they are 0.388, 0.236, 0.188, for m = 1, 2, 3, respectively.

When the thin phase grating is nonsinusoidal, the theoretical formulation is not straightforward as each order diffraction is composed of contributions of waves from other order harmonic gratings, which interfere constructively or destructively. However, when the higher order grating components, δn_2, δn_3, etc, are much smaller than δn_1, the contribution from the first order grating dominates all interfering contributions from the higher order gratings. This is not the situation reflected in our experimental data (Figure 3), where the first order diffraction is much stronger than the higher order ones and time behaviors of all diffractions are significantly different from one another. Large values of the higher order grating components and resultantly strong interferences by them might be assumed to explain Figure 3. However, this assumption cannot explain why the first order diffraction can be described well by a sum of exponential functions.

The above speculations deny the thin phase grating limit since each multiple diffraction in our signals is not likely to couple with one another. This condition can be achieved under the Bragg condition that is important as the grating thickness becomes intermediate or thick limit.[19-20] Under the Bragg condition, only the m-th order harmonic grating contributes to the m-th order diffraction.[21] When the modulation depth is small, the intensity of the m-th order diffraction is approximately proportional[18b,19a] to $\sin^2\gamma_m$ or δn_m^2. There-

fore, we can deduce relative values of $|\delta n_m|$ from the measured intensities of each order diffractions.

The application of the Bragg condition when the excitation depth is similar with the fringe spacing of the grating might seem inappropriate. However, the thin grating forms only during times earlier than a few microsecond as the heat dissipation into the front glass is that fast, while major transient dynamics in Figure 3 takes place in millisecond regime. The initial thin thermal grating triggers the reordering processes which are much slower and take place over the whole sample thickness, providing the condition under which the Bragg condition is applicable.

C. Simulations. If the grating shape is purely sinusoidal, only the first order diffraction is generated under the Bragg condition.[15,19] The observation of the higher order diffractions implies that the laser-induced grating is out of the sinusoidal shape. The time-varying refractive index modulation function, $\Delta n(x, t)$ can be expressed following Eq. (3a) as

$$\begin{aligned}\Delta n(x,t) = {} & \delta n_1(t)[\cos(qx)+1] \\ & + \delta n_2(t)[\cos(2qx+\phi_2)+1] \\ & + \delta n_3(t)[\cos(3qx+\phi_3)+1] \\ & + \cdots + \text{ terms independent of } x\end{aligned} \tag{3b}$$

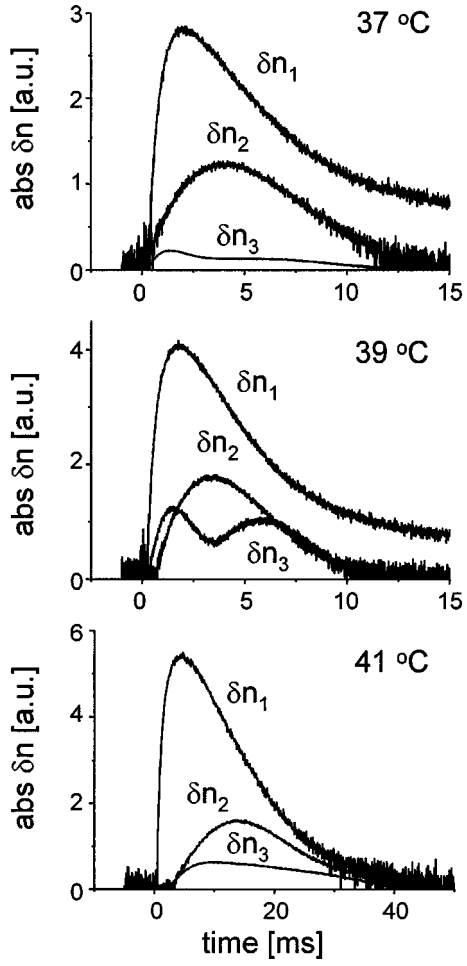

Figure 4. The time evolution of $|\delta n_m|$'s determined from the data of Figure 3. The early spikes due to the second component were removed in the data treatment.

In the followings, we will consider the gratings only up to the third order, as the ignorance of the fourth and higher orders results in an error less than 1%. Since the signal intensity of each order diffraction is proportional to the square of the corresponding δn_m, we can determine the absolute values of δn_m's from the diffraction signals shown in Figure 3. The time evolutions of $|\delta n_m|$'s are shown in Figure 4. The early spikes by the second component are removed in the experimental data treatment. In order to determine the modulated refractive index of the medium, Δn, the signs of the δn_m's and the relative phases ϕ_m's should be known. The higher order gratings must be in phase or out of phase with respect to the first order grating since each order grating must conserve symmetry; that is, the relative phase is either 0 or π. There are 32 cases of the different δn_m's and ϕ_m's when the gratings up to the third order are considered. However, some cases give the same grating shapes with constant refractive index shifts. For example, the second order grating with the positive refractive index change δn_2 and the phase $\phi_2 = 0$ has the same shape as the grating with the negative δn_2 and $\phi_2 = \pi$. These gratings have the constant difference of $2\delta n_2$. The constant difference of the modulated refractive index, which is included in the "terms independent of x" in Eq. (3b), does not contribute to the diffraction of the signal. The second and the third order gratings give two different grating shapes, respectively. Therefore, 8 cases should be considered as the possible grating shapes.

The anisotropy of the nematic phase shows two refractive indices, the ordinary (n_o) and the extraordinary (n_e) ones, depending on the relative geometry of the molecular alignment and the polarization of the incident light. The n_e is involved in our experimental geometry[12,22] and the n_e of nematic MBBA decreases with the temperature rise in the nematic phase as does the refractive index of the isotropic phase.[13] Therefore, overall change of the refractive index during the dynamics should be negative when the temperature rises and/or the melted state is formed. The initial refractive index of the bright peak part of the grating should be smaller than that of the dark null part, that is, $\Delta n(qx = 0) < \Delta n(qx = \pi)$. Since the absolute values of initial δn_m's are in the order of $|\delta n_1| > |\delta n_2| > |\delta n_3|$ as shown in Figure 4, the cases with the negative δn_1 can be considered for the possible grating profile.

We simulate the following four cases with Eq. (3b) and the δn_m's shown in Figure 4 to investigate the evolution of the grating shape. The constant "terms independent of x" are not considered.

Case A. $\delta n_1(t) < 0$, $\delta n_2 > 0$, $\phi_2 = 0$, $\delta n_3 > 0$, $\phi_3 = 0$.
Case B. $\delta n_1(t) < 0$, $\delta n_2 > 0$, $\phi_2 = 0$, $\delta n_3 > 0$, $\phi_3 = \pi$.
Case C. $\delta n_1(t) < 0$, $\delta n_2 > 0$, $\phi_2 = \pi$, $\delta n_3 > 0$, $\phi_3 = 0$.
Case D. $\delta n_1(t) < 0$, $\delta n_2 > 0$, $\phi_2 = \pi$, $\delta n_3 > 0$, $\phi_3 = \pi$.

When the positive quantities are used for δn_m's, the following expressions are obtained for above cases.

Case A. $\Delta n(x, t) = -\delta n_1(t)[\cos(qx) + 1] + \delta n_2(t)[\cos(2qx) + 1] + \delta n_3(t)[\cos(3qx) + 1]$

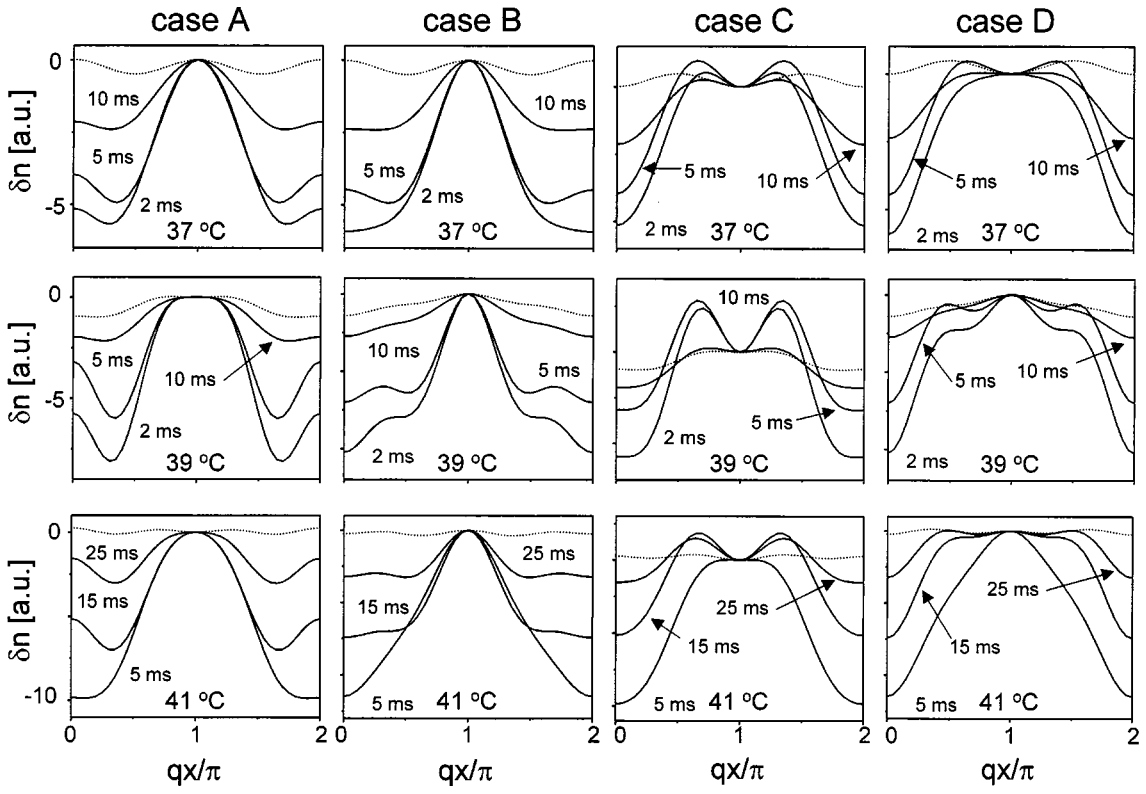

Figure 5. The simulated grating shapes for cases A, B, C and D at 37, 39 and 41 °C.

Case B. $\Delta n(x, t) = -\delta n_1(t)[\cos(qx) + 1] + \delta n_2(t)[\cos(2qx) + 1] + \delta n_3(t)[-\cos(3qx) + 1]$

Case C. $\Delta n(x, t) = -\delta n_1(t)[\cos(qx) + 1] + \delta n_2(t)[-\cos(2qx) + 1] + \delta n_3(t)[\cos(3qx) + 1]$

Case D. $\Delta n(x, t) = -\delta n_1(t)[\cos(qx) + 1] + \delta n_2(t)[-\cos(2qx) + 1] + \delta n_3(t)[-\cos(3qx) + 1]$

The simulation results are shown in Figure 5. The center of the diagram, $qx = \pi$ corresponds to the null of the grating, and the edges ($qx = 0$ and 2π) correspond to the peak of the grating. Since the "terms independent of x" of Eq. (3b) change with time but work as a constant off-set in the refractive index modulation, the simulated results are adjusted with the constant to be zero at the grating null. The dotted line represents the refractive index at $t = 0$ ms and reflects the noise of the data. While the displayed ordinate range is slightly different in each diagram, the same amount of interval is covered in the diagrams of each temperature. Refer the delay times to the dynamic change of the refractive index in Figure 4.

Each case of Figure 5 reveals the main spatial position which causes the deviation of the grating shape from the sinusoid. In case A, the deviation makes the refractive index at the peak change less than that between the peak and the null. In case B, the refractive index of the peak changes faster than that of the null. The intial shape around the null is kept longer. In case C, the refractive index of the position between the peak and the null changes faster than that of the null. The refractive index of the null becomes smaller than around during the dynamics. In case D, the refractive index around the null changes faster than that of the peak to reach the equilibrium. The overall grating shape change indicates the faster modulation of the refractive index occurs around the null rather than around the peak. It should be noted that the "terms independent of x" of Eq. (3b) are not considered here, that is, the refractive index change of Figure 5 is not the absolute change but the relative difference between the peak and the null.

Since the refractive index of MBBA changes linearly with temperature in the nematic and the isotropic phases as mentioned previously, the refractive index profile can be regarded as the temperature profile of the sample. Therefore, in cases A and C, the temperature does not evolve smoothly between the null and the peak; that is, there is a bump in the temperature profile. This kind of temperature profile is not physically acceptable. In case B, the temperature changes faster at the null at the peak than at the null while the temperature changes faster at the null in case D. When it is considered that the sample is sandwiched between glass plates whose thermal conductivity is much greater than that of MBBA, it is reasonable that the temperature changes faster at the peak position with the greater temperature gradient. That is, case B, where $\delta n_1(t) < 0$, $\delta n_2 > 0$, $\phi_2 = 0$, $\delta n_3 > 0$, $\phi_3 = \pi$, is regarded as the physically acceptable temperature profile. Of course, the following cases give the same results as case B; $\delta n_1(t) < 0$, $\delta n_2 < 0$, $\phi_2 = \pi$, $\delta n_3 > 0$, $\phi_3 = \pi$; $\delta n_1(t) < 0$, $\delta n_2 > 0$, $\phi_2 = 0$, $\delta n_3 < 0$, $\phi_3 = 0$; $\delta n_1(t) < 0$, $\delta n_2 < 0$, $\phi_2 = \pi$, $\delta n_3 < 0$, $\phi_3 = 0$. However, it is not possible to choose one case as correct because the absolute refractive index including "the terms independent of the position" can not be deter-

mined from the diffraction signals.

D. Nature of the melted state. The slower dynamics at higher nematic temperatures can be understood with the phase transition of the sample, which is closely related to the phototransformed state, or the locally melted state. As mentioned in the introduction section, the isotropic phase of the liquid crystalline materials is different from the conventional isotropic liquid because of the pseudonematic domains which are maintained up to the temperatures well above the nematic-isotropic transition temperature, T_{NI}. The correlation length of the pseudonematic domain ξ is given by[2]

$$\xi = \xi_o[T^*/(T-T^*)]^{1/2} \quad (5)$$

where ξ_o is on the order of the molecular dimension and T^* is a temperature slightly below T_{NI}. At the nematic phase, $T < T_{NI}$, the correlation length becomes infinite. The pseudonematic domain is regarded as being maintained up to the temperature where $\xi = 3\xi_o$. For MBBA, T^* is found to be 46.4 ^oC and the pseudonematic domain is maintained up to 82 ^oC.[5] The pseudonematic domains introduced into the sample by laser-induced local melting give a great effect on the diffraction signals via the order parameter fluctuation - disorder-reorder process.

For the nematic liquid crystals, the refractive index change due to the thermal fluctuation, Δn^{th} can be given by three terms as[22]

$$\Delta n^{th} = \delta n_T + \delta n_\rho + \delta n_S \quad (6)$$

where each term corresponds to the pure temperature contribution (δn_T), the density fluctuation (δn_ρ), and the order parameter fluctuation (δn_S). In the above equation, the pure temperature fluctuation term can be neglected. The density fluctuation moving at the speed of sound should be resolved in the time scale of nanosecond. The fluctuation of the order parameter gives a large effect on the signal of the millisecond time scale. The local order parameter does not vanish even after the transition from the nematic phase to the isotropic phase as long as the temperature jump is not greater than 40 degrees. The exact estimation of the laser-induced temperature jump under our experimental conditions is a quite difficult task with the complex heat conduction by the glass wall and the strong absorption condition. However, the temperature jump is estimated to be much less than 40 degree.[12] Even though the temperature jump is greater than 40 degree, the following discussion would not be affected much. The dynamic change into the region where the pseudonematic domain vanishes would occur at the time scale of millisecond.

The slower dynamics at 41 ^oC than at lower temperatures indicates that the phase transition into the isotropic phase occurs and the order parameter fluctuation by the pseudonematic domains undergoes at the sample of 41 ^oC. The disorder-reorder process involved in the phase transition is slower than the disorder-reorder process in the nematic phase. The sample at 39 ^oC seems to be at the border of reaching the phase transition by the laser-induced temperature jump, as is consistent with the previous estimations.[12] It should be noted that the thermal effect of the refractive index discussed above can be induced by the local fluctuation and that the temperature dependence of the multiple order diffractions may be interpreted as the scale difference of the produced pseudonematic domains.

Conclusions

We used the laser-induced transient grating method to separate dynamically the physical origins of the optical nonlinearity of a liquid crystal. When this method is applied to the nematic MBBA under the strong absorption condition, the four distinguishable physical origins are found in the time range of microseconds to milliseconds; the thermal diffusion, the reordering induced by the temperature perturbation, the reordering induced by the phototransformed state, and the mass diffusion of the photoisomer. While the full analysis is found in our previous paper,[12] we presented the additional higher order diffraction experiments to study the nature of the phototransformed state, which gives the dominant feature for the extraordinarily high optical nonlinearity. The possible grating shapes are reproduced from the intensities of the multiple order diffractions and the physically acceptable grating shape is discussed. The pseudonematic domain, which gives the non-vanishing local order parameter for the isotropic phase, is responsible for the phototransformed state to reveal the reordering dynamics in the time scale of millisecond.

Acknowledgments. This work was supported by NON-DIRECT RESEARCH FUND (01-D-0587), Korea Research Foundation and by the grants from the Basic Science Research Institute (BSRI-97-3432).

References

1. Chandrasekhar, S. *Liquid Crystals*, 2nd ed.; Cambridge University Press: Cambridge, 1992.
2. de Gennes, P. G.; Prost, J. *The Physics of Liquid Crystals*, 2nd ed.; Clarendon Press: Oxford, 1993.
3. (a) Khoo, I.-C.; Wu, S.-T. *Optics and Nonlinear Optics of Liquid Crystals*; World Scientific: Singapore, 1993. (b) Khoo, I.-C. *Liquid Crystals*; John Wiley & Sons: New York, 1995.
4. *Liquid Crystals for Advanced Technologies*; Bunnings, T. J., Chen. S. H., Kajiyama, T., Koide, N., Eds.; Materials Research Society: Pittsburgh, 1996.
5. (a) Deeg, F. W.; Greenfield, S. R.; Stankus, J. J.; Newell, V. J.; Fayer, M. D. *J. Chem. Phys.* **1990**, *93*, 6303. (b) Stankus, J. J.; Torre, R.; Fayer, M. D. *J. Phys. Chem.* **1993**, *97*, 9478.
6. Choi, M.; Jin, D.; Kim, H.; Kang, T. J.; Jeoung, S. C.; Kim, D. *J. Phys. Chem. B* **1997**, *101*, 8092.
7. Hsiung, H.; Shi, L. P.; Shen, Y. R. *Phys. Rev. A* **1984**, *30*, 1453.
8. Khoo, I. C.; Shepard, S. *J. Appl. Phys.* **1983**, *54*, 5491.
9. (a) Khoo, I. C.; Normandin, R. *J. Appl. Phys.* **1984**, *55*, 1416. (b) Khoo, I. C.; Normandin, R. *IEEE J. Quantum Electron.* **1985**, *QE-21*, 329.
10. Eichler, H. J.; MacDonald, R. *Phys. Rev. Lett.* **1991**, *67*,

2666.
11. Jin, D.; Kim, H.; Kim, S. H.; Kim, S. K. *J. Phy. Chem. B* **1997**, *101*, 10757.
12. Yoon, B. H.; Kim, S. H.; Lee, I.; Kim, S. K.; Cho, M.; Kim, H. J. *Phys. Chem. B* **1998**, *102*, 7705.
13. Shen, J.; Clark, N. A.; Pershan, P. S.; Priestly, E. B. *J. Chem. Phys.* **1977**, *66*, 4635.
14. Koren, G. *Phys. Rev. A* **1976**, *13*, 1177.
15. Eichler, H. J.; Günter, P.; Pohl, D. W. *Laser-Induced Dynamics Grating*; Springer-Verlag: Berlin, 1986.
16. Kim, S. H.; Kim, S. K. *Bull. Korean Chem. Soc.* **1996**, *17*, 365.
17. Pinkevich, I. P.; Reznikov, Yu. A.; Reshetnyak, V. Yu.; Yaroshchuk, O. V. *Int. J. Nonlinear Opt. Phys.* **1992**, *1*, 447.
18. (a) Magnusson, R.; Gaylord, T. K. *J. Opt. Soc. Am.* **1978**, *68*, 806. (b) Magnusson, R.; Gaylord, T. K. *J. Opt. Soc. Am.* **1978**, *68*, 809.
19. (a) Su, S. F.; Gaylord, T. K. *J. Opt. Soc. Am.* **1975**, *65*, 59. (b) Magnusson, R.; Gaylord, T. K. *J. Opt. Soc. Am.* **1977**, *67*, 1165.
20. Kogelnik, H. *Bell. Syst. Tech. J.* **1969**, *48*, 2909.
21. This condition holds as long as the modulation depth is small and the grating is not too thick. Our experimental conditions are well within these limits. See reference 19 for detailed parameters of these limits.
22. Terazima, M. *Bull. Chem. Soc. Jpn.* **1996**, *69*, 1881.